DARK MATTER MAY NOT BE SO DARK: Testing Massive Primordial Black Hole Dark Matter with Galactic X-Ray Emission

Honors Thesis

By

Nolan McPhaul

Under the advisement of Dr. Kelly-Holley Bockelmann

In partial fulfillment of the requirements for the honor degree of

Bachelor of Arts in Physics

Submitted April 16, 2024

Abstract

Were Primordial Black Holes (PBHs) to exist, they could constitute a significant portion of dark matter in our universe which could be explored through gravitational wave emission, gravitational lensing, and electromagnetic observations. Assuming PBHs as a dark matter candidate, we determine the X-ray emission they would radiate from accreting gas in their host galaxy by modelling the dark matter particles in the Romulus25 cosmological simulation as clusters of PBHs. Upon simulating such emission, we compare our X-Ray luminosity functions to those derived from observations with the Chandra X-Ray Telescope to constrain the abundance of PBHs compared to dark matter as a function of PBH mass spanning $10^{-2} - 10^{5} M_{\odot}$. Our results highly constrain the most massive PBHs but leave a vast sea of stellar and sub-stellar mass PBHs unscathed by falling under the flux limitations of Chandra. Therefore, further studies are needed in such a mass regime to explore the possibility of PBHs as a considerable source of dark matter and black holes in our universe. The implications of such could have drastic impacts on our understanding of the composition, machinations, and evolution of our universe.

Acknowledgements

I cannot extend enough gratitude to my thesis advisor, Professor Kelly-Holley Bockelmann, for her persistent guidance, advice, and corny humor through this entire experience. You have been my North Star through the past two years here and none of this would have been possible without you. Thank you! I would also like to thank the members of my thesis committee: Professor Scherrer, Professor Varga, and Professor Taylor for taking the time to help in a crucial part of my journey in reviewing my thesis, being great professors, and offering amazing advice.

Contents

Chapter 1

Introduction & Background

1.1. What are Primordial Black Holes?

Primordial black holes (PBHs) are a theoretical family of black holes formed from the gravitational collapse of the primordial curvature power spectrum shortly after inflation. Generating in clusters called massive PBHs (MPBHs) during the radiation era, such PBHs could initially range from 10^{-21}-10^{5} $M_{\odot}$, peaking around planetary masses; however, over the billions of years since their formation into the present day they would have merged and accreted surrounding matter to grow into masses primarily ranging from $0.01 - 10^{5}$ $M_{\odot}$, with the most massive reaching over 10^{9} $M_{\odot}$ as measured from supermassive black holes in the centers of massive galaxies, [5].

Were these MPBHs to be prevalent enough in our universe, it could be tied to the origin of supermassive and intermediate mass black hole seeds in the early universe, drive early galactic and stellar evolution, produce the gravitational wave signals observed by LIGO-Virgo-KAGRA, create a stochastic background of gravitational waves, as well as provide sources for some of the most energetic events in our universe including X-ray binaries (XRBs) and ultraluminous X-ray sources (ULXs) visible in nearby galaxies, as well as seeding the massive black holes in active galactic nuclei (AGN) [7].

1.2. How are they Related to Dark Matter?

Despite its vast importance in making up 85% of the matter in our universe which is undetectable through electromagnetic observations, the origin of dark matter is still left largely unknown. While most research into possible candidates has focused on subatomic particles such as weakly interacting massive particles and axions, others have proposed dark stars, cosmic strings, massive compact halo objects (MACHOs), and other astrophysical objects to explain the gravitational observations of dark matter from galaxies and dense stellar clusters.

Therefore, were PBHs to exist in our universe they would have to represent a portion of dark matter since they would be a source of mass previously unrepresented in the measurements from electromagnetic emission of galaxies, which could have vast implications on the composition of matter in our universe. As such, past and current research into the possibilities of PBHs as a dark matter candidate have placed many constraints on the theory which are represented in Figure 1.1 as upper limits on the fraction of dark matter able to be modeled as PBHs, which is referenced as the abundance of PBHs from here on. Most famous of these constraints is the MACHO project's conclusion that less than 10% of the dark matter in the Milky Way halo can consist of objects over 10 $M_{\odot}$, as the gravitational lensing experiment would have detected the effects of such massive, compact objects, [2]. Such limitations have resulted in the theory we analyze from [7] which is represented by the black line in the figure for the abundance of PBHs they believe to be most likely given current observational constraints. One can see that such a theory could allow for the majority of dark matter to persist through PBHs while passing MACHO's stringent limit of less than 10% being made of PBHs above 10 $M_{\odot}$.

While the theory allows for much of dark matter to be made of PBHs, we take a more conservative approach and wish to further constrain limits on the possible abundance of PBHs in our universe to further develop such an impactful theory.

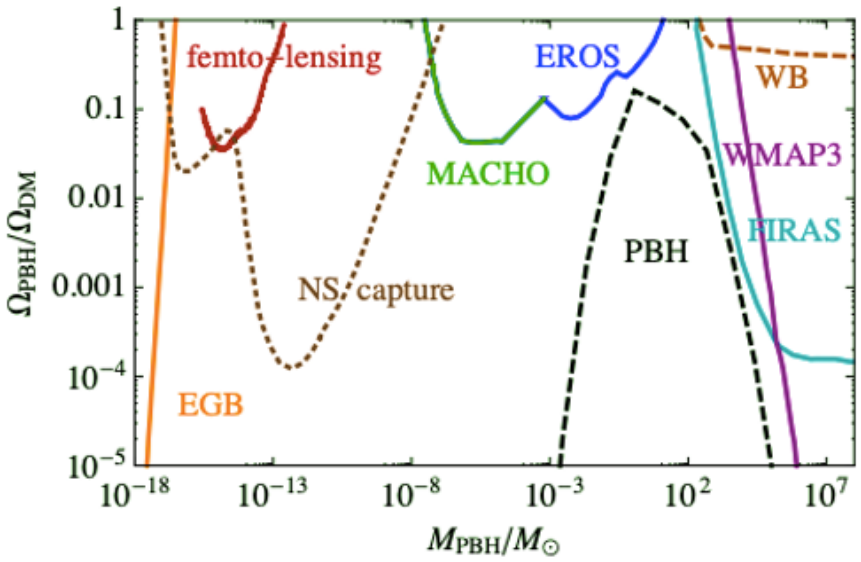

Figure 1.1: Limits on the abundance of PBHs in the universe today. The dashed black line represents the particular scenario described in [7] within limitations. The limits come from analyses on the effect of PBHs on the extragalactic photon background (orange), gravitational fento-lensing (red) and micro-lensing (green and blue), neutron star capture in globular clusters (dark brown), stripping of wide binaries (light brown), and the CMB through FIRAS (cyan) and WMAP3 (purple). Figure is referenced from [7].

1.3. How Could We See Them?

Were PBHs to constitute a significant portion of dark matter in our universe then they would be spread throughout galaxies roughly following the same distribution as dark matter observations. This would place many PBHs and their corresponding MPBHs in gas dense regions where the cluster would begin to accrete this local gas material. Such a process would produce significant accretion in the X-ray band, since this is the primary emission type for stellar mass black holes, which could be observed by telescopes such as the Chandra X-Ray Observatory if the source is both luminous and close enough.

Were this emission to be observed, is is likely that such observations would be classified as an X-ray binary (XRB) which is traditionally classified as a compact object (in this case a black hole) accreting its bound companion star. This type

of X-ray emission is classified into two categories depending on the mass of the companion star being accreted: low-mass X-ray binaries (LMXBs) which have bursts of emission from a companion star of $< 10\ M_\odot$ and high-mass X-ray binaries (HMXBs) which emit steady pulses from the accretion of a companion star $\geq 10\ M_\odot$ [13].

Recent research has demonstrated power law relations between the the number and type of XRBs and the properties of its host galaxy, with the number of LMXBs in a halo correlating with its stellar mass ($M_\star$) while the number of HMXBs correlates with the star formation rate (SFR) of its host galaxy, as demonstrated in [9], [10], and [15].

In our analysis we analyze the X-ray emission of PBHs as they accrete local gas material in the $z = 0.00$ snapshot from Romulus25. We then compare our results against models from observations of HMXBs and LMXBs against the stellar mass and SFR of the MPBH's host galaxy. From such we derive additional constraints on the abundance of PBHs ranging from $10^{-2} - 10^5\ M_\odot$. Through this work, we help constrain PBHs as a possibility for explaining the observations of dark matter and introduce additional signatures of PBHs which should be observed were they to constitute enough dark matter in our universe.

This thesis is laid out as follows. In Chapter 2 we outline how we analyze the local gas properties to find the accretion rate of each MPBH in the simulation, how we find the X-ray luminosities given such accretion rates, and then how we classify our X-ray sources into HMXB and LMXB components. In Chapter 3 we discuss properties of our X-ray population and conclude with the constraints we place on the abundance of PBHs by comparing our X-ray population to local observation of XRBs.

Chapter 2

Methods: Bringing Dark Matter to Light

In this chapter we demonstrate our process for modeling the X-ray emission from the halos in our simulation. Specifically, we detail how we seed the MPBHs as dark matter, find the properties of local gas particles, produce a density cut for more accurate accretion, as well as how we derive and classify our X-ray luminosities from the MPBH's accretion rate, along with the $M_\star$ and SFR of the host halo.

2.1. Modeling PBHs as Dark Matter in Romulus25

2.1.1 Halo Sample Selection

Since we are analyzing the accretion of local gas particles onto MPBHs were they to represent a portion of dark matter, we only analyze halos in Romulus containing at least one gas particle. This gives us a population of 25,198 halos out of the original 103,222 halos in the snapshot to analyze.

For our results on the accretion rates and X-ray luminosity values for our model we use this halo population; however, when we compare our model against observations we only do so for the sample of 349 halos with $M_\star > 10^9 M_\odot$ and

$0.05 <$ SFR ($M_\odot$/ yr) < 6 as used in [9] for their observational sample. This is because traditional XRB sources have been found to correlate with the $M_\star$ and SFR of their host galaxy, so observers traditionally only analyze the most massive and highest star forming galaxies to find the most X-ray sources for population studies.

2.1.2 MPBH Dark Matter Model

For a high enough spatial resolution to analyze PBH dark matter against standard ΛCDM models, as postulated in [7], we used the Romulus25 simulation. For a more detailed description of the Romulus suite of cosmological simulations see [14]; however, we proceed to describe the relevant properties for our research.

Romulus25 is a cosmological hydrodynamic simulation run with N-body + the smoothed particle hydrodynamics (SPH) code CHANGA, to accurately evaluate galactic evolution out to high redshifts inside a (25 Mpc)^3 volume of the universe. With its Plummer-equivalent force softening of 250 pc, we are able to better resolve dark matter and gas particles for more accurate dynamics and analysis of gas properties. Such a high resolution allows for the simulation to contain dark matter particles with a mass of 3.39 x $10^5\,M_\odot$ and gas particles with masses of 2.12 x $10^5\,M_\odot$. Further, the dark matter particles being less massive than most other cosmological SPH simulations allows for Romulus25 to contain 3.375 times more dark matter particles than gas, whereas most simulations have equal number of gas and dark matter particles. This allows us to use Romulus25 to better resolve our MPBHs and better simulate their accretion of local gas particles for more realistic and accurate results. The simulations were run with a Planck 2014 ΛCDM cosmology, with $\Omega_0 = 0.3086$, $\Lambda = 0.6914$, $h = 0.67$, and $\sigma_8 = 0.77$, [1].

Throughout our analysis we calibrate simulated stellar masses using corrections from [11] to account for observations missing some stars in their search (especially those far from the center of the halo) which create differences such that $M_{\star,Obs} = 0.6\,M_{\star,Sim}$. With these corrections, Romulus is able to resolve galaxies down to $M_\star > 10^7 M_\odot$, so these are the limits to the types of halos we are able to analyze in our study.

In our analysis we have two quantities which we vary: the mass of individual PBHs (M_{PBH}) whose upper limit is the mass of dark matter particles in the

simulation, and the abundance of such PBHs (n_{PBH}) which ranges from 0-1 and represents the fraction of dark matter we are modeling as PBHs. We proceed by treating all dark matter particles as MPBHs which contain PBHs of equal mass, resulting in the number of PBHs within a MPBH being modeled as $N_{PBHs} = M_{DM}/M_{PBH}$. We then scale the abundance of PBHs for what percent of each dark matter particle is being modeled as PBHs such that the true number of PBHs in every dark matter particle is given by

$$N_{PBHs} = \frac{n_{PBH} * M_{DM}}{M_{PBH}} \tag{2.1}$$

where M_{DM} is the mass of every dark matter particle in the simulation.

By analyzing the dark matter particles in this manner, we evaluate the maximum abundance of PBHs at each mass value to provide the most conservative constraint from our analysis.

2.2. Accretion of Local Gas

2.2.1 Accretion Model

For our analysis we use Bondi-Hoyle accretion as it is a good approximation for these PBHs accreting through a sea of gas, for a more in depth review of this model see [4]. For our purposes we consider the MPBH moving through or past multiple gas particles which are made almost entirely of hydrogen gas and which are accreted onto the individual PBHs according to the following,

$$\dot{M}_{PBH} = \frac{4\pi G^2 M_{PBH}^2 \rho_\infty}{(c_\infty^2 + v_\infty^2)^{3/2}} \tag{2.2}$$

where $\dot{M}_{PBH}$ is the accretion rate onto a single PBH, ρ_∞ is the local gas density, c_∞ is the speed of sound in the gas (otherwise denoted as c_s), and v_∞ is the relative velocity of the gas to the black hole.

For the speed of sound and the relative velocity we use the following equations,

$$c_s = \sqrt{\frac{\gamma R T_k}{M}} \tag{2.3}$$

$$v_\infty^2 = |v_{DM} - v_{Gas}|^2 \tag{2.4}$$

where $\gamma = 5/3$ is the adiabatic index of hydrogen gas, $R = 8.31\ J/mol * K$ is the gas constant, T_k is the gas temperature in kelvin, and M is the molecular mass of hydrogen gas which we take to be $M = 0.59259$ x 10^{-3} kg/mol from the Romulus25 parameter file.

Since we are analyzing the collective MPBH emission rather than that of individual PBHs, we sum over the $\dot{M}_{PBH}$s in the cluster; however, since we assume equal PBH masses and equal accretion among each PBH in the cluster we can simply say

$$\dot{M}_{MPBH} = N_{PBHs} * \dot{M}_{PBH} \tag{2.5}$$

which in combining Equations 2.1 and 2.5 we derive our final equation for the accretion of gas onto the MPBH cluster to be

$$\begin{aligned} \dot{M}_{MPBH} &= N_{PBHs} \frac{4\pi G^2 M_{PBH}^2 \rho_\infty}{(c_\infty^2 + v_\infty^2)^{3/2}} \\ &= (\frac{n_{PBH} M_{DM}}{M_{PBH}}) \frac{4\pi G^2 M_{PBH}^2 \rho_\infty}{(c_\infty^2 + v_\infty^2)^{3/2}} \\ &= n_{PBH} M_{DM} \frac{4\pi G^2 M_{PBH} \rho_\infty}{(c_\infty^2 + v_\infty^2)^{3/2}} \\ &= \beta\ n_{PBH} M_{PBH} \end{aligned} \tag{2.6}$$

From Equation 2.6 we can see that for the purpose of our analysis $\dot{M}_{MPBH}$ only depends linearly on the mass and abundance of PBHs in the cluster, with the constant β containing the local gas properties of each MPBH and the mass of each dark matter particle. Therefore, once we solve for β (which means finding the local density, temperature, and velocity of gas) for each dark matter particle we can scale M_{PBH} and n_{PBH} until our results no longer agree with observations, which will provide a new constraint curve on the abundance versus mass plot such as those shown in Figure 1.1.

2.2.2 Finding Local Gas Properties

To find the accretion rate of our MPBHs, we have to solve for the density, temperature, and velocity of local gas particles which are being accreted by the

MPBH cluster. To determine the best representation of the local gas material near each MPBH we tested two main methods: using the properties of the nearest gas particle versus averaging such over the nearest 32 gas particles (which is the more traditional approach as in [14] & [12]). The latter method was further divided into 2 types of weighted averages based on the distance from a quadratic and a smoothing kernel density estimation (KDE) to give a more accurate representation of the accretion which should primarily affect the closest gas particles.

To estimate the effectiveness of each method we compared the accretion rates to the local gas density which is displayed in Figure 2.1 for a particular halo with $M_{PBH} = 50\ M_{\odot}$ & $n_{PBH} = 1$.

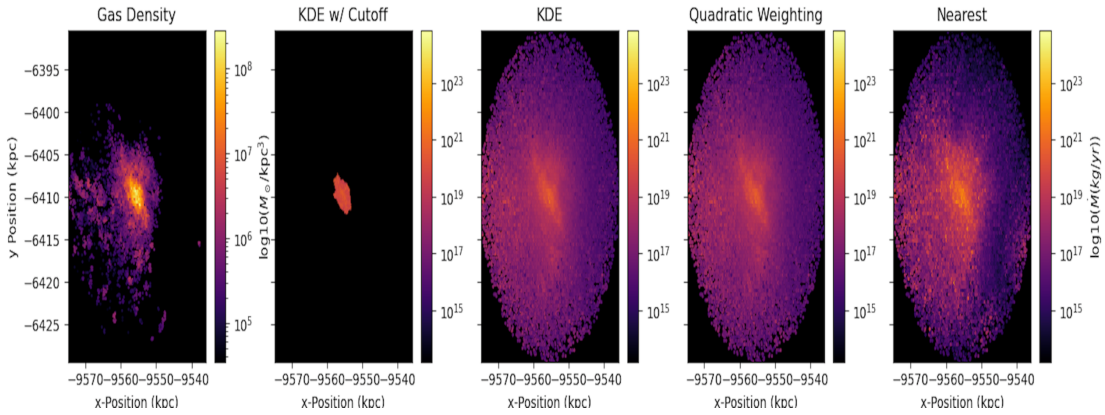

Figure 2.1: From left to right we display the gas density map and our MPBH accretion rates from 4 methods of deriving local gas properties: KDE with a density cutoff, KDE smoothing over nearest 32 gas particles, quadratic weighting over the nearest 32 gas particles, and the nearest gas properties.

From the figure one can see that the accretion method which best aligns with the gas density map is the KDE estimate; however, many of the accreting MPBHs are in areas without any gas at all. Upon further inspection of a large sample of halos in our snapshot, we realized that the KDE was not accurately describing the local gas properties but was simply smoothing over the nearest 32 gas particles regardless of how far they were from the MPBH source, resulting in MPBHs accreting in areas without any gas present.

Therefore, to accurately model the accretion of only local gas particles, we added the criteria to only count a MPBH as accreting if all 32 gas particles were

within 2 softening lengths (500 pc) which is the method displayed in the 2nd panel of Figure 2.1. From this criteria, we reduced the portion of MPBHs accreting from every MPBH to only around 4% as actively accreting which aligned the best with the densest gas regions of the halos. Since each gas particle in the simulation is around the same mass (2.12 x $10^5\ M_\odot$), this essentially created a density cutoff to select MPBHs in gas dense areas above $\rho_{Gas} \geq \frac{32 M_{Gas}}{\frac{4}{3}\pi(500pc)^3} = 1.3$ x $10^7\ M_\odot/\text{kpc}^3$ which is seen in Figure 2.1.

Therefore, since our KDE method with the density cutoff provided the best accuracy of accretion rates compared to local gas density, this is what we use to derive all of our accretion rates and ultimately our luminosities from here on.

2.3. PBH Luminosities

2.3.1 Deriving the MPBH X-Ray Luminosity

Now with our accurate accretion rates for the relevant MPBHs in the snapshot, we can derive the bolometric luminosity of such clusters using the Eddington Luminosity equation

$$L_{Bol} = \eta c^2 \dot{M}_{MPBH} \tag{2.7}$$

with radiative efficiency η=0.1 for black holes (where η represents what fraction of the rest energy being accreted per second is emitted from the system, which for black holes has a 10% efficiency).

Once we have the bolometric luminosity we can easily find what percent is emitted in X-rays through the bolometric correction (BC) of XRB systems which can vary by the accretion rate of the black hole as in [3], but tend to stay around 0.6-0.9 for X-ray bands in the 0.5-10 keV range. Therefore, we chose $BC = 0.8$ to analyze the X-ray emission in the 0.5-10 keV band for a more conservative estimate of the total X-ray luminosity we could detect. This therefore brings the X-ray luminosity (L_X) as $L_X = BCL_{Bol}$, shown more completely as

$$L_X = BC\eta c^2 \dot{M}_{MPBH} \tag{2.8}$$

which when combined with Equation 2.6 is equivalent to

$$L_X = BC\eta c^2 \beta \; n_{PBH} M_{PBH} \tag{2.9}$$

relying on constants and our two primary variables: the abundance of dark matter being modeled as PBHs (n_{PBH}) and the mass of each individual PBH (M_{PBH}). Therefore we can easily find the luminosity values across our parameter space by scaling our initial values of n_{PBH} and M_{PBH}. In doing such we begin our analysis using $n_{PBH} = 1$ and $M_{PBH} = 50 M_\odot$ as [7] believed this to be a possible regime which was previously not tested. Therefore, all of the images, statistics, and data given are for this particular model unless otherwise stated.

2.3.2 Classifying LMXB & HMXB Sources

In our analysis we compare to observations from [9] of the host galaxy's stellar mass and star formation rate to identify which of our simulated halos were best for observational comparison. We easily calculate the halo's stellar mass as the sum of each star particle's mass; however, for the SFR we had to subjectively determine which method was best. To derive our SFR we used the mass of stars born within a specific age cutoff. In analyzing multiple age cutoffs we determined 100 Myr to be the best value for our halos in question since it was the cutoff used in [9] to determine their SFR values and agreed well between our simulated halos and observations.

This gave us a sample of 349 halos whose MPBH X-ray sources were decomposed into their respective LMXB and HMXB components based on the specific-star formation rate ($sSFR = SFR/M_\star$) of their host galaxy. Observations from [8], [9], and [10] have shown that galaxies with sSFR $> 10^{-10}$ yr^{-1} are almost exclusively dominated by HMXBs while those with lower sSFR are dominated by LMXB sources. Therefore we claim all MPBH X-ray sources in halos above this limit to be HMXB while those from galaxies with a lower sSFR are all LMXBs. Thus giving us 134 halos with HMXB sources and 215 halos with LMXB sources. We use this sample in our comparisons against observations as described in Sec. 3.2.

Chapter 3

Results and Discussion: A Bright Future from a Bright Past

In this chapter, we analyze our population of MPBH X-ray sources. We derive basic statistics about our X-ray population and compare the X-ray emission from some of our most massive and highest star forming galaxies against observations from local galaxies. We conclude with our constraints on the feasible abundance of PBHs in our universe which we limit through the amount of X-ray emission such PBHs should emit were they to represent a significant portion of dark matter.

3.1. MPBH XRB Population

With our derived X-ray luminosities of the 25,198 halos containing gas particles, we derived statistics for the following distribution of X-ray luminsoties for $M_{PBH} = 50M_{\odot}$ and $n_{PBH} = 1$ as shown in Figure 3.1.

Each halo has on average 4% of its dark matter particles actively accreting as MPBHs, generating an average emission of $10^{36} \pm 10^{37}$ erg/s. For reference, the luminosities of HMXBs and LMXBs range from around $10^{35} - 10^{40}$ erg/s, peaking at around $10^{37} - 10^{39}$ erg/s and $10^{36} - 10^{37}$ erg/s respectively. Sources above 10^{39} erg/s are known as ultra-luminous X-ray sources which from Figure 3.1 you can see MPBH could be candidates of, while some of the most energetic X-ray emission events in the universe are from active galactic nuclei which can emit up to 10^{48} erg/s.

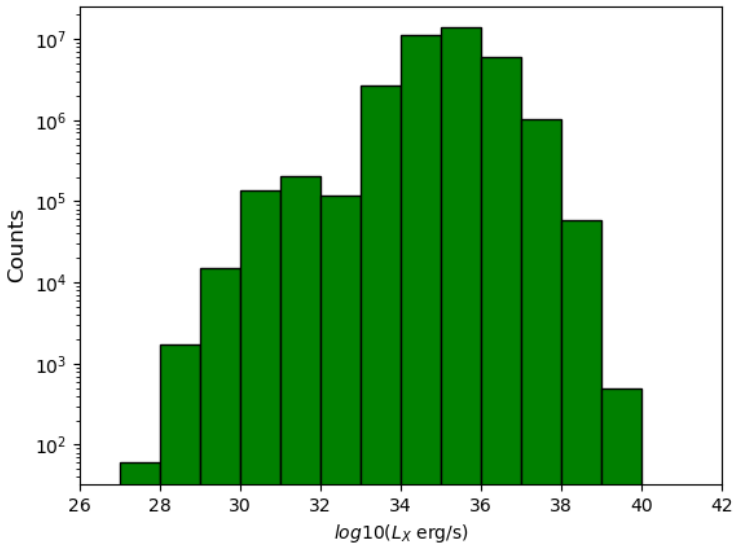

Figure 3.1: Distribution of luminosities from our population of 25,198 halos for $M_{PBH} = 50M_{\odot}$ and $n_{PBH} = 1$.

For comparisons against the stellar emission of galaxies and for better localization of our MPBH sources we further analyzed the population of 7,798 halos containing dark matter, gas, and stars. We have plotted our luminosities compared to the stellar emission averaged over all bands and the gas density of 3 halos in Figure 3.2.

As you can see, the density cutoff caused for the accreting MPBHs to lie in the densest gas regions which mostly occur in the central galaxy within the main halo or in any pockets of gas such as orbiting or infalling subhalos. Therefore, as opposed to most PBH search methods which consist of examining the surrounding dark matter halos of galaxies, our results allow for additional constraints to be placed from observations of the central galaxy itself. Such localization of X-ray sources could be used to differentiate between PBH and traditional XRB emission or other sources of X-ray emission from the galaxy (through stars, gas, or an AGN) given enough angular resolution of nearby X-ray sources for such a localization within the host galaxy.

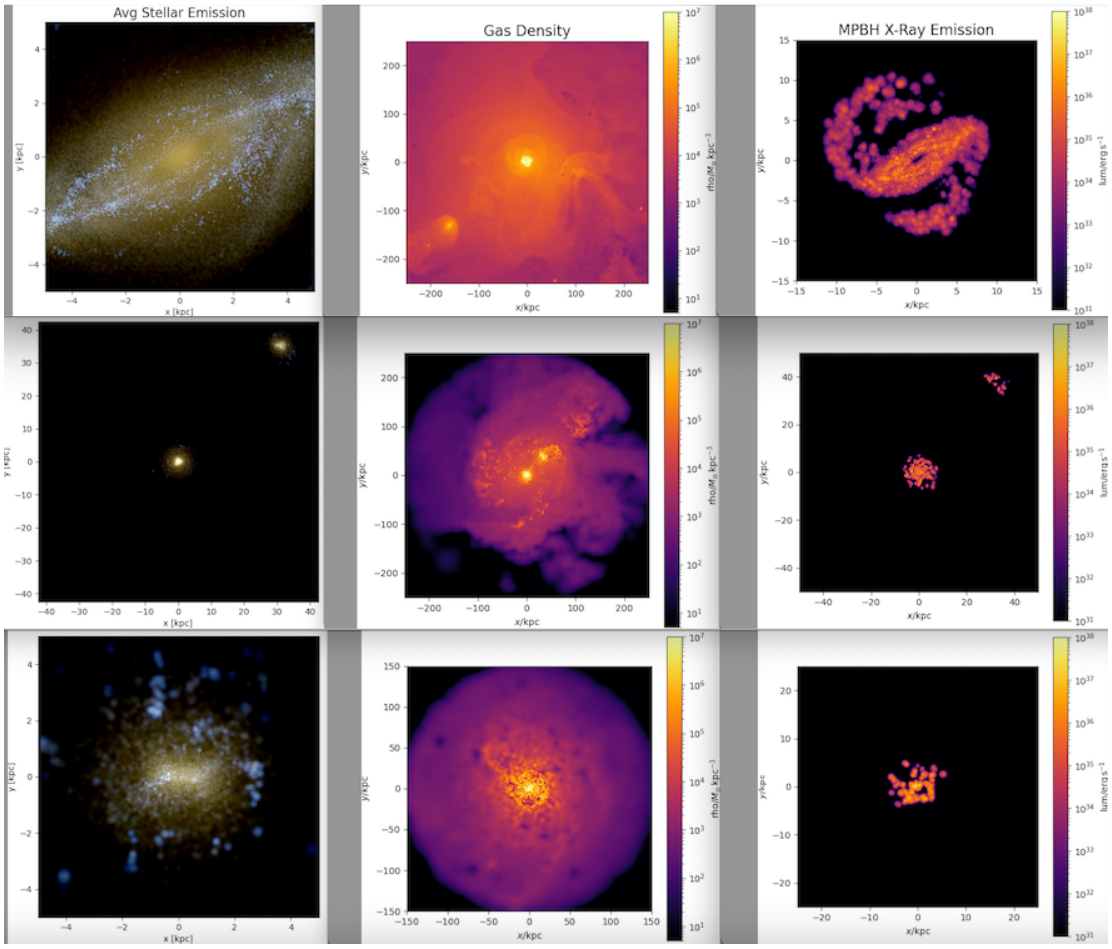

Figure 3.2: The stellar luminosity averaged over all bands (column 1), gas density (column 2), and MPBH X-ray emission (column 3) for 3 halos are shown. The 3 rows represent halos at $M_\star \approx 5\text{x}10^{11} M_\odot$, $M_\star \approx 5\text{x}10^{10} M_\odot$, and $M_\star \approx 5\text{x}10^{9} M_\odot$ respectively. We scaled the MPBH luminosity plots to demonstrate their positions almost exclusively in the galaxy and not the surrounding gas or dark matter halos.

3.2. Comparing against XRB Observations

To compare our model to observations we use the halo selection and XRB decomposition into LMXB and HMXB components from [9] and as decribed in Sec. 2.1.1 and Sec. 2.3.2 respectively. With our model for the X-ray emission of accreting MPBHs in each halo we compared our results to the X-ray luminosity functions (XLFs) for HMXBs and LMXBs from [9] as shown in Figure 3.3.

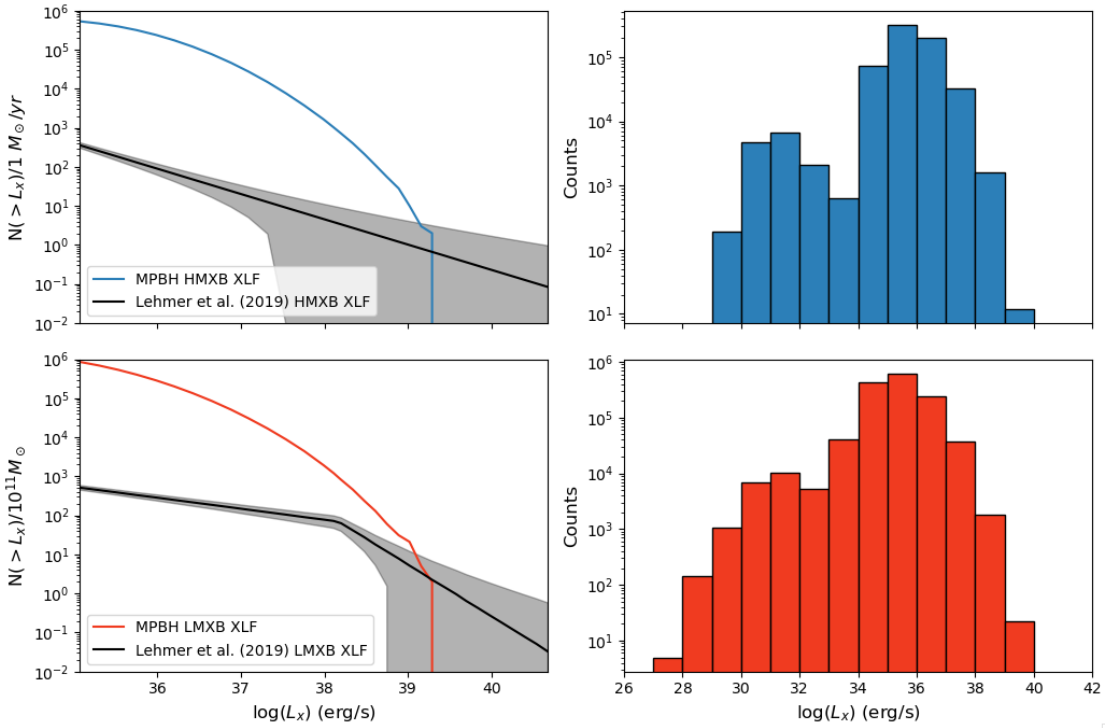

Figure 3.3: XLFs (left panels) and their corresponding histograms (right panels) for our HMXBs (top row) and LMXBs (bottom row) at $M_{PBH} = 50M_\odot$ and n_{PBH}=1. The y-axis, $N(> L_X)$, represents the number of sources from our entire population above a given luminosity (from the x-axis), which is normalized by the total SFR for our HMXB population and $M_{\star,Total}/10^{11}M_\odot$ for our LMXB population as these sources have been shown to correlate with SFR and $M_\star$ repspectively. The black curves represent the models from [9] for HMXBs (top left panel) and LMXBs (bottom left panel) with their respective $\pm 3\sigma$ errors shown in the grey shaded region.

From Figure 3.3 you can see whether or not our models agree with XRB observations by whether or not the colored curves are inside or below the observational limits demonstrated by the grey shaded area around the black curve. Since the

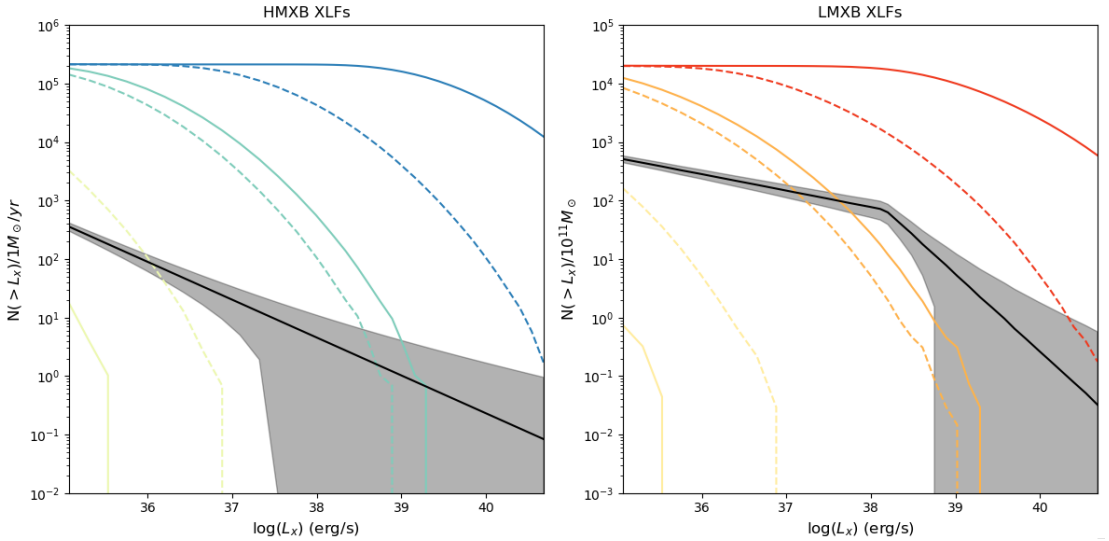

Figure 3.4: Above we show the XLFs for our MPBH HMXBs (left panel) and LMXBs (right panel) for various M_{PBH} and n_{PBH} values across our parameter space. For both panels, the solid lines represent XLFs of varying masses at $n_{PBH} = 1$ while the dashed lines represent XLFs of varying abundances at $M_{PBH} = 2{,}000\ M_\odot$. Starting from the bottom left and working to the top right of both graphs we have $(M_{PBH}(M_\odot),\ n_{PBH}) = (0.01, 1),\ (2000, 10^{-4}),\ (2000, 10^{-2}),\ (50, 1),\ (2000, 1),$ and $(250000, 1)$. Only the HMXB (0.01,1) along with the LMXB (0.01,1) and (2000,10^{-4}) curves are feasible since these are the only XLFs which fall under observations and therefore would not be observed as a distinct population of MPBH XRBs apart from stellar origin XRBs.

black curves represent the observed relations of HMXBs and LMXBs which agree well with the XRB population synthesis predictions from [6], we do not propose to replace traditional stellar evolution XRB populations purely with XRBs from MPBHs, but rather we propose both populations could exist together to explain most X-ray observations. This is why we only consider our MPBH XRB model given M_{PBH} and n_{PBH} initial conditions to be consistent with X-ray observations if the emission from our MPBHs is less than that from XRBs, demonstrated by our colored XLF curves falling below their respective observational XLFs (as shown in black).

To test our models across the available mass and abundance parameter space, we use the linear scaling relations of M_{PBH} and n_{PBH} on the X-ray luminsoity from each MPBH as shown in Equation 2.9. In doing such, we are able to find the

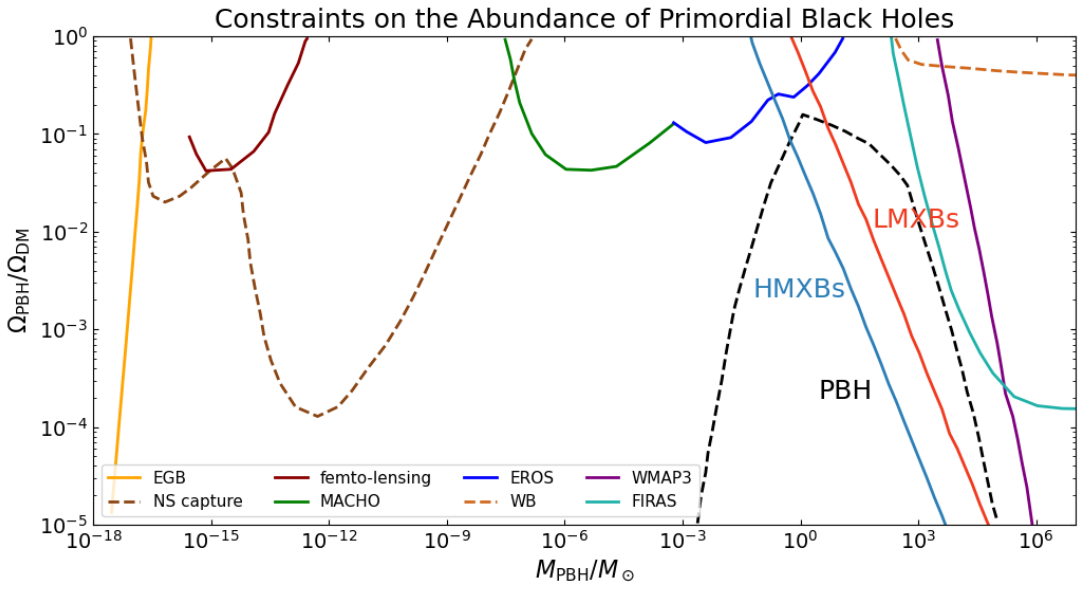

Figure 3.5: Here we show our final results for what abundance of dark matter can feasibly be modeled as PBHs for various mass values which we have adapted from [7]. The curves represent upper limits, where abundances above such would have been observed from the listed techniques. The model which we base our assumptions on from [7] is shown as the dashed black line labeled PBH. Our results for HMXBs and LMXBs are shown respectively in the blue and red curves labelled as such. Therefore, our results constrain much of the original model as we would have seen the X-ray emission of such PBHs were they to exist.

X-ray luminosities for MPBHs across our mass and abundance parameter space as shown in Figure 3.4 where we compare three M_{PBH}s at $n_{PBH} = 1$ (shown as the solid curves in both panels) and three n_{PBH} values at $M_{PBH} = 2,000 M_\odot$ (shown as the dashed curves in both panels).

From such, we are able to scale our parameters as shown in Figure 3.4 and compare the results to the observed XLFs as in Figure 3.3 to constrain the M_{PBH} and n_{PBH} values for our models which fall below the observational limits. By doing such across our entire parameter space we were able to derive constraint curves from our modeled emission of HMXBs and LMXBs as shown in Figure 3.5 as the blue and red lines, respectively.

Chapter 4

Conclusion

Since dark matter represents over 85% of the matter in our universe, it is crucial for us to understand and model this illusive source of mass to understand everything form the birth of galaxies, to their structure and evolution, and possibly to the composition of gas, stars, and black holes. Therefore, our analysis of PBHs as a candidate of dark matter is able to help further the goal of understanding the composition of matter in our universe.

In modeling dark matter from the Romulus25 simulations as MPBHs we are able to track the accretion and X-ray luminosity of each dark matter particle were it to be a cluster of PBHs. From such we model our X-ray luminosity counts as a function of the luminosity and compare such against population studies of local galactic X-ray observations. This allows us to derive our final constraint curve from modelling PBHs as HMXB and LMXB sources of X-ray emission.

Caveats of this methodology include whether or not the CHANDRA X-Ray Observatory would be able to spatially resolve individual PBHs or if it would see each MPBH as a point source of X-ray emission. Were the resolution good enough, then the methods used to conclude our final results would have to change to individial, resolved PBHs rather than the X-ray emission from the entire PBH cluster. However, given the distance to many of the galaxies observed in X-ray studies, we believe this to be a good assumption for modelling the emission as a point source from the entire MPBH to derive conservative constraints on the abundance of PBHs.

Our results are able to constrain M_{PBH}s from 10^{-2} to 10^{5} $M_{\odot}$ and n_{PBH} from

1 to less than 10^{-5} meaning the most massive PBHs we modelled at $M_{PBH} > 1000\ M_{\odot}$ cannot constitute more than 0.001% of dark matter in our universe. These constraints of the highest mass PBHs are important for future electromagnetic and gravitational wave experiments which hope to observe black holes in this mass range to explain the origin of intermediate mass black holes in our universe and their relation to seeding supermassive black holes and driving galactic evolution. However, while our results highly constrain massive PBHs, the possibility for a sea of stellar and sub-stellar PBHs is left open to discovery and scrutiny by further studies.

References

[1] Ade, P. A. R., and et. al. Planck 2015 results: Xiii. cosmological parameters. *Astronomy amp; Astrophysics 594* (Sept. 2016), A13.

[2] Alcock, C., and et. al. Eros and macho combined limits on planetary-mass dark matter in the galactic halo. *The Astrophysical Journal 499*, 1 (may 1998), L9.

[3] Anastasopoulou, K., Zezas, A., Steiner, J. F., and Reig, P. Average bolometric corrections and optical to x-ray flux measurements as a function of accretion rate for x-ray binaries. *Monthly Notices of the Royal Astronomical Society 513*, 1 (Apr. 2022), 1400–1413.

[4] Bondi, H., and Hoyle, F. On the mechanism of accretion by stars. *104* (Jan. 1944), 273.

[5] Clesse, S., and García-Bellido, J. Massive primordial black holes from hybrid inflation as dark matter and the seeds of galaxies. *Physical Review D 92*, 2 (July 2015).

[6] Fragos, T., Lehmer, B., Tremmel, M., Tzanavaris, P., Basu-Zych, A., Belczynski, K., Hornschemeier, A., Jenkins, L., Kalogera, V., Ptak, A., and Zezas, A. X-Ray Binary Evolution Across Cosmic Time. *764*, 1 (Feb. 2013), 41.

[7] García-Bellido, J. Massive primordial black holes as dark matter and their detection with gravitational waves. *Journal of Physics: Conference Series 840* (May 2017), 012032.

[8] Lehmer, B. D., Alexander, D. M., Bauer, F. E., Brandt, W. N., Goulding, A. D., Jenkins, L. P., Ptak, A., and Roberts, T. P. A Chandra Perspective on Galaxy-wide X-ray Binary Emission and its Correlation with Star Formation Rate and Stellar Mass: New Results from Luminous Infrared Galaxies. *724*, 1 (Nov. 2010), 559–571.

[9] Lehmer, B. D., Eufrasio, R. T., Tzanavaris, P., Basu-Zych, A., Fragos, T., Prestwich, A., Yukita, M., Zezas, A., Hornschemeier, A. E., and Ptak, A. X-ray binary luminosity function scaling relations for local galaxies based on subgalactic modeling. *The Astrophysical Journal Supplement Series 243*, 1 (June 2019), 3.

[10] Mineo, S., Gilfanov, M., and Sunyaev, R. X-ray emission from star-forming galaxies - i. high-mass x-ray binaries: Hmxbs in star-forming galaxies. *Monthly Notices of the Royal Astronomical Society 419*, 3 (Nov. 2011), 2095–2115.

[11] Munshi, F., Governato, F., Brooks, A. M., Christensen, C., Shen, S., Loebman, S., Moster, B., Quinn, T., and Wadsley, J. Reproducing the stellar mass/halo mass relation in simulated cdm galaxies: Theory versus observational estimates. *The Astrophysical Journal 766*, 1 (mar 2013), 56.

[12] Sharma, R. S., Brooks, A. M., Tremmel, M., Bellovary, J., Ricarte, A., and Quinn, T. R. A hidden population of massive black holes in simulated dwarf galaxies. *The Astrophysical Journal 936*, 1 (Sept. 2022), 82.

[13] Tan, C. High-mass x-ray binary: Classification, formation, and evolution. *Journal of Physics: Conference Series 2012*, 1 (sep 2021), 012119.

[14] Tremmel, M., Karcher, M., Governato, F., Volonteri, M., Quinn, T. R., Pontzen, A., Anderson, L., and Bellovary, J. The romulus cosmological simulations: a physical approach to the formation, dynamics and accretion models of smbhs. *Monthly Notices of the Royal Astronomical Society 470*, 1 (May 2017), 1121–1139.

[15] Zhang, Z., Gilfanov, M., and Bogdán, Á. Dependence of the low-mass X-ray binary population on stellar age. *546* (Oct. 2012), A36.